THE JOURNAL OF PHYSICAL CHEMISTRY B

Article

Cite This: J. Phys. Chem. B XXXX, XXX, XXX−XXX

pubs.acs.org/JPCB

# Smart Hybrid Nanocomposite for Photodynamic Inactivation of Cancer Cells with Selectivity

*Published as part of The Journal of Physical Chemistry virtual special issue "Hai-Lung Dai Festschrift".*

Jeong-Wook Hwang,[†,⊥] Seung-Jin Jung,[†,⊥] Taek-Chin Cheong,[‡,§,⊥] Yuri Kim,[‡,§,⊥] Eon Pil Shin,[†] Il Heo,[†] Gwanghun Kim,[‡,§] Nam-Hyuk Cho,[*,‡,§] Kang-Kyun Wang,[*,†] and Yong-Rok Kim[*,†]

[†]Department of Chemistry, Yonsei University, 50 Yonsei-ro, Seodaemun-gu Seoul 03722, Republic of Korea

[‡]Department of Microbiology and Immunology, Seoul National University College of Medicine, 103 Daehak-ro, Jongno-gu Seoul 03080, Republic of Korea

[§]Department of Biomedical Sciences, Seoul National University College of Medicine, 103 Daehak-ro, Jongno-gu Seoul 03080, Republic of Korea

Supporting Information

**ABSTRACT:** Photodynamic therapy has been efficiently applied for cancer therapy. Here, we have fabricated the folic acid (FA)- and pheophorbide A (PA)-conjugated FA/PA@$Fe_3O_4$ nanoparticle (smart hybrid nanocomposite, SHN) to enhance the photodynamic inactivation (PDI) of specific cancer cells. SHN coated with the PDI agent is designed to have selectivity for the folate receptor (FR) expressed on cancer cells. Structural characteristics and morphology of the fabricated MNPs were studied with X-ray diffraction and scanning electron microscopy. The photophysical properties of SHN were investigated with absorption, emission spectroscopies, and Fourier transform infrared spectroscopy. In addition, the magnetic property of $Fe_3O_4$ nanoparticle (MNP) can be utilized for the collection of SHNs by an external magnetic field. The photofunctionality was given by the photosensitizer, PA, which generates reactive oxygen species by irradiation of visible light. Generation of singlet oxygen was directly evaluated with time-resolved phosphorescence spectroscopy. Biocompatibility and cellular interaction of SHN were also analyzed by using various cancer cells, such as KB, HeLa, and MCF-7 cells which express different levels of FR on the surface. Cellular adsorption and the PDI effect of SHN on the various cancer cells *in vitro* were correlated well with the surface expression levels of FR, suggesting potential applicability of SHN on specific targeting and PDI of FR-positive cancers.

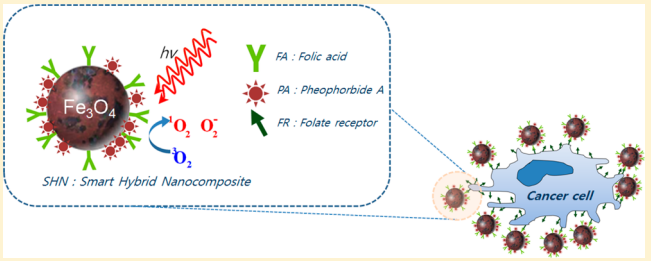


## INTRODUCTION

Photodynamic therapy (PDT) is an effective medical method to treat various cancers by inducing cell necrosis and apoptosis with reactive oxygen species (ROS).[1−3] It has been considered as a new strategy against the traditional invasive treatment for various cancers because it is relatively noninvasive and efficiently eradicates cancers.[4,5] Since PDT was approved in 1993 to treat cancer in Canada, several countries have used PDT as an alternative method to conventional cancer treatments.[6,7]

There are several requirements for the ideal PDT. The light absorbing agent of a photosensitizer (PS) must selectively be localized in the tumor tissue, and the cell toxicity only emerges with the light irradiated to destroy the cancer cells without affecting normal cells.[8] The selective localization of PS is important to minimize the side effect on the normal cells.[9] However, the lack of selective targeting of PS to cancer tissues is one of the major obstacles for improving the efficiency of photodynamic inactivation (PDI).[10] In order to solve such a limitation, many experiments have been performed for the selective PDI using the photosensitizers directly conjugated with a receptor or an antibody.[11−15] Among the target-oriented PDI reagents, photofunctional carriers conjugated with/without targeting molecules have extensively been studied by many researchers.[16−18] A photodynamic inactivation process using PDI reagent based on nanoparticles is usually consistent with the general PDI process with PS. In particular, the photosensitizing nanoparticles show more effective PDI efficiency than the free photosensitizer molecules due to the enhanced permeability and retention effect (EPR) in cancer tissues.[19,20]

However, the photofunctional carriers conjugated with/without targeting molecules for a specific cancer cell can be aggregated due to the composition of a protein corona on the surface of the carriers.[21,22] The corona layer on the surface of the carriers may also suppress the ROS generation by PDI

Received: May 7, 2019
Revised: July 16, 2019
Published: July 16, 2019







DOI: 10.1021/acs.jpcb.9b04301
J. Phys. Chem. B XXXX, XXX, XXX−XXX

reagent and decrease the cellular adsorption efficiency because of the modification of intrinsic properties of the carrier regarding of structure, size, shape, and surface polarity.[23−25] Among the intrinsic properties of the carrier, the surface polarity and the size uniformity might be major determinants for the efficiency of photodynamic therapy since these properties can affect the interaction of the carriers with specific cancer cells.[26−28] Therefore, to develop efficient target-oriented photodynamic reagents, PDI reagents have to be designed and fabricated with consideration of ROS generation efficiency, cytotoxicity, the stability of surface polarity, and size uniformity.

In this study, we report the therapeutic possibility of a smart hybrid nanocomposite (SHN) for folate-receptor-positive cancer cells. The $Fe_3O_4$ nanoparticle (MNP) utilized in this study was widely used in a biomedical field due to low cytotoxicity, good biocompatibility, uniform dispersion property, and stability in a biological environment.[29−32] For the photoinduced and targeting functionalization of MNP, PA and FA were covalently bonded to the surface of MNP by the esterification reaction in this study. Additionally, the selective adsorption and cytotoxicity of SHN against FR-positive cancer cells were evaluated *in vitro*.

## EXPERIMENTAL METHODS

**Fabrication of Smart Hybrid Nanoparticle (SHN).** MNPs were prepared using the solvothermal reduction method as described previously.[33] MNPs were dispersed in THF (Merck, HPLC grade) containing PA (10 mL, $5 \times 10^{-5}$ M, Frontier Scientific, 95%) and then agitated (200 rpm) at room temperature for 24 h to fabricate SHNs by a wet chemical process. After the reaction, the products were washed with THF solvent five times to remove the residual PA and then dried at 60 °C. After 6 h, the PA-conjugated MNPs were added to a DMSO (Merck, HPLC grade) solution containing FA (10 mL, $4.36 \times 10^{-6}$ M, Sigma-Aldrich, 97%). It was agitated at room temperature for 24 h under dark conditions. Finally, the mixture was placed on a magnet to remove the unreacted FA. FA-conjugated PA@MNPs were then washed with the DMSO solution three times.

**Characterization of Smart Hybrid Nanoparticles (SHNs).** Field emission scanning electron microscopy (FE-SEM, 7800F, JEOL) was used for the characterization of MNP morphology.[34] The crystallographic structure of MNP was confirmed with an X-ray diffractometer (XRD, Ultima IV, Rigaku) working on Cu K$\alpha$ radiation.[35] To study the photophysical properties of SHNs, an FT-IR (Vertex 70), a UV−vis spectrophotometer (U-2900, Hitachi), and a spectrofluorometer (F-2500, Hitachi) were utilized.[34] The singlet oxygen generation from SHNs was confirmed with the time-resolved spectroscopic method. The nanosecond Nd:YAG (surelite II-10, Continuum) pumped optical parametric oscillator laser (OPO plus, Continuum) was used for the excitation source ($\lambda_{ex}$ = 668 nm).[34] The near-infrared photomultiplier tube (NIR-PMT, H10330A; Hamamatsu) and monochromator (DMC1-05, Optometrics) were utilized to detect the time-resolved singlet oxygen phosphorescence signal. To avoid light scattering from SHNs, the cutoff (<1000 nm; CVI) and the interference filters (1270 nm, Spectrogon) were both placed before the entrance slit of the monochromator.[35] The photoluminescence signals were amplified and acquired by an amplifier (SR445A, Stanford Research Systems) and a digital oscilloscope (DS07052A, Agilent Technology). After incubating SHNs in Dulbecco's Modified Eagle Medium (DMEM, Welgene) containing 10% fetal bovine serum (FBS) solution for 24 h at 37 °C, zeta potential and hydrodynamic diameter of SHNs were measured with a zeta potential analyzer (NanoZS, Malvern) and a DLS analyzer (ELS-1000ZS, Otsuka), respectively.[36,37]

**Biological Assays.** The FR-positive (KB and HeLa) and FR-negative (MCF-7) cells were purchased from American Type Culture Collection (ATCC). Mouse embryonic fibroblasts (MEF) were prepared from embryos at E13.5 as described previously[38] and used as primary control cells. The cells were cultured and maintained in complete DMEM supplemented with 10% heat-inactivated FBS in humidified 5% $CO_2$ atmosphere at 37 °C.[39] Expression of folate receptor on the cell surface was analyzed by flow cytometry after staining with mouse antifolate receptor antibody and Alexa488 goat anti-mouse IgG (Abcam).[40] KB, HeLa, and MCF-7 cells ($1 \times 10^5$ cells/mL) were incubated with 1 mL of DMEM supplemented with 10% FBS and SHNs, PA@MNP, or PA for 1 h at 37 °C under dark condition. Cells were then washed with ice-cold PBS supplemented with 1% bovine serum albumin (MP Biomedicals) and 1 mM EDTA (Sigma-Aldrich) three times.[41] The efficiency of MNP or PA uptake to cells was measured by flow cytometry (BD, FACS Canto II) right after incubation, and the data were analyzed by Flowjo 10.6.0 software. Cytotoxicity of SHN on various cells was evaluated by using an MTT assay kit (Sigma-Aldrich) according to the manufacturer's instruction. For the photodynamic tumoricidal activity assay *in vitro*, a light-emitting diode (LED; $\lambda_{max}$= 658 nm, full-width at half-maximum = 70 nm, 6.6 mW/cm$^2$) was utilized as an irradiation light source with a cutoff filter (<400 nm; CVI) for blocking the residual UV light from the LED. A total power output of the irradiation was measured using a laser power meter (THORLABS, PM200). Experiments of photodynamic tumoricidal activity were performed with various concentrations of PA and PA@ $Fe_3O_4$ to compare with the efficacy of SHN. The number of PA molecules bonded to the surface of $Fe_3O_4$ nanoparticles was estimated using UV−vis absorption spectroscopy. Absorption optical densities (ODs) at 668 nm were measured with the initial PA/THF solution ($5.0 \times 10^{-5}$ M) before the addition of magnetic particles for reaction and also with the PA/THF solution that remained after reaction with the particles. The OD difference between the initial and the remaining PA/THF solutions indicated that $\sim 8.0 \times 10^{-8}$ mol (equivalent to $4.8 \times 10^{16}$ molecules) of PA was immobilized onto the surface of 10 mg of $Fe_3O_4$. Therefore, the number of PA molecules bonded to the surface of the magnetic particles at 25, 50, 100, and 200 $\mu$g/mL of SHN was equivalent to the number of PA molecules in the liquid solution at concentrations of 0.2, 0.4, 0.8, and 1.6 $\mu$M, respectively. The cells treated with MNP or PA were exposed to the LED light for 10 min and then incubated at 37 °C for 24 h in a dark humidified incubator. After the incubation, the viability of cells was assessed by MTT assay.[42,43]

**Statistical Analysis.** The data were analyzed using Graph Pad Prism 5.01 software (GraphPad Software). Statistical analysis was performed using one-way analysis of variance (ANOVA) followed by Tukey's multiple comparison test. Data are expressed as the mean ± standard deviation. A $p$-value of <0.05 was considered statistically significant.



DOI: 10.1021/acs.jpcb.9b04301
J. Phys. Chem. B XXXX, XXX, XXX−XXX

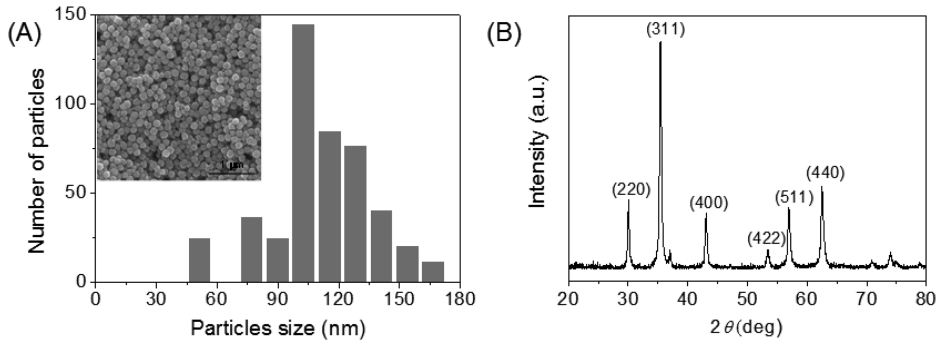


**Figure 1.** (A) Particle size distribution of MNPs and scanning electron microscope (SEM) image (inset) and (B) X-ray diffraction (XRD) pattern of MNPs.

## RESULTS AND DISCUSSION

The fabricated MNPs revealed good size uniformity as shown in Figure 1A. The size distribution of MNPs was evaluated by 400 particles in different fields of the SEM images. The average diameter of MNPs is 110 ± 23 nm. The powder XRD pattern of the MNPs provides more detailed structural information as shown in Figure 1B. The strong Bragg peaks ($2\theta$ = 30.0°, 35.6°, 43.3°, 53.7°, 57.0°, 62.8°) are marked by their Miller indices ((220), (311), (400), (422), (511), and (440)).[44] It was well-correlated to the standard $Fe_3O_4$ powder diffraction data (JCPDS 19-0629). This also shows that the magnetite crystal structure of the fabricated MNPs is a cubic inverse spinel.[44]

FT-IR spectra of FA, FA@MNPs, PA, and SHNs were compared to understand the bonding nature of PA and FA to the surface of the MNPs (Figure 2). IR spectrum of the pure

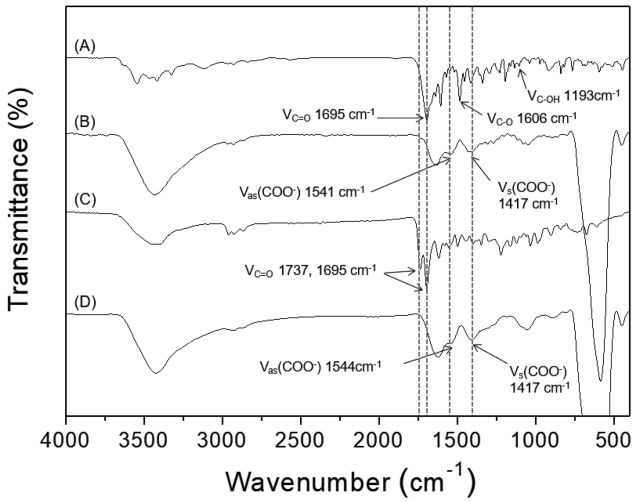


**Figure 2.** FT-IR spectra of (A) FA, (B) FA@MNPs, (C) PA, and (D) SHNs.

FA shows the absorption peaks at 1695, 1606, and 1193 $cm^{-1}$. These peaks originated with the stretching modes of the free carbonyl double bond ($\nu_{C=O}$), the carbon−oxygen single bond ($\nu_{C-O}$), and the OH deformation ($\nu_{C-OH}$), respectively.[45] Therefore, these peaks suggest that FA has the protonated carboxyl groups (COOH). In addition, the peaks at 1541 and 1417 $cm^{-1}$ in the IR spectrum of the FA bonded to the surface of MNPs can be assigned to the asymmetric ($\nu_{as}$) and the symmetric ($\nu_s$) stretch vibrations modes of the carboxylate group, respectively.[45,46] This implies that the carboxyl group is conjugated to the Fe ion of MNP as mentioned in a previous study.[47] The FT-IR spectrum of the pure PA shows the absorption peaks at 1693 and 1737 $cm^{-1}$, which correspond to the stretching vibration modes of the free carbonyl double bond ($\upsilon_{C=O}$). These peaks disappeared after the conjugation of PA to the surface of MNPs. Moreover, the new absorption peaks appear at 1544 and 1411 $cm^{-1}$, potentially due to the coordination of Fe ions on MNP by carboxylic acids of PA as reported in a previous study.[48]

In Figure 3A, the spectrum of PA in THF solution shows one B band (410 nm) and four Q bands (504, 534, 608, and 666 nm). The absorption spectrum of SHNs in THF solution also includes the B and Q bands at the same wavelength. The emission peaks of SHNs in THF solution at 675 and 725 nm are similar to those of PA in THF solution at the excitation of 410 nm, as shown in Figure 3B. This may imply that the photophysical properties of PA are not significantly altered by the bonding of PA and MNP.[48] The time-resolved singlet oxygen phosphorescence signals were measured in THF solution at the detection wavelength of 1270 nm and shown in Figure 3C,D. Singlet oxygen phosphorescence signals from the samples are fitted with a single exponential decay function, resulting in the similar singlet oxygen lifetimes of 21.7 and 22.1 $\mu$s for PA and SHN, respectively. The lifetimes correspond well to the results observed in the previous studies.[49−53] This further suggests that the singlet oxygen generated from SHNs has not been influenced by either MNP or the FA and PA molecules conjugated on the surface of MNP.

In order to assess the biocompatibility of the synthetic SHNs, various cancer cells including KB, HeLa, and MCF-7 cells were incubated with different amounts of SHNs in DMEM containing 10% FBS under the dark condition. We also included a primary cell, MEF, as a noncancerous control (Figure 4A). SHN itself was barely toxic to the cancer cell types in the concentration range 0−200 $\mu$g/mL. On the other hand, SHN was slightly toxic to MEFs and reduced the viability by ∼20% at the high concentration (>100 $\mu$g/mL). These results suggested that optimization of SHN concentration is required for *in vivo* application to minimize the side effect of SHN. Nevertheless, the surface polarity of SHNs was constant in the DMEM containing 10% FBS for 24 h as shown in Figure 4B. To check the size stability of SHNs in the DMEM containing 10% FBS, hydrodynamic diameters of SHNs were measured with DLS analyzer. Figure 4C shows that there has been no significant size change of SHNs although the size of SHNs was initially increased to near 200 nm. The initial


DOI: 10.1021/acs.jpcb.9b04301
J. Phys. Chem. B XXXX, XXX, XXX−XXX

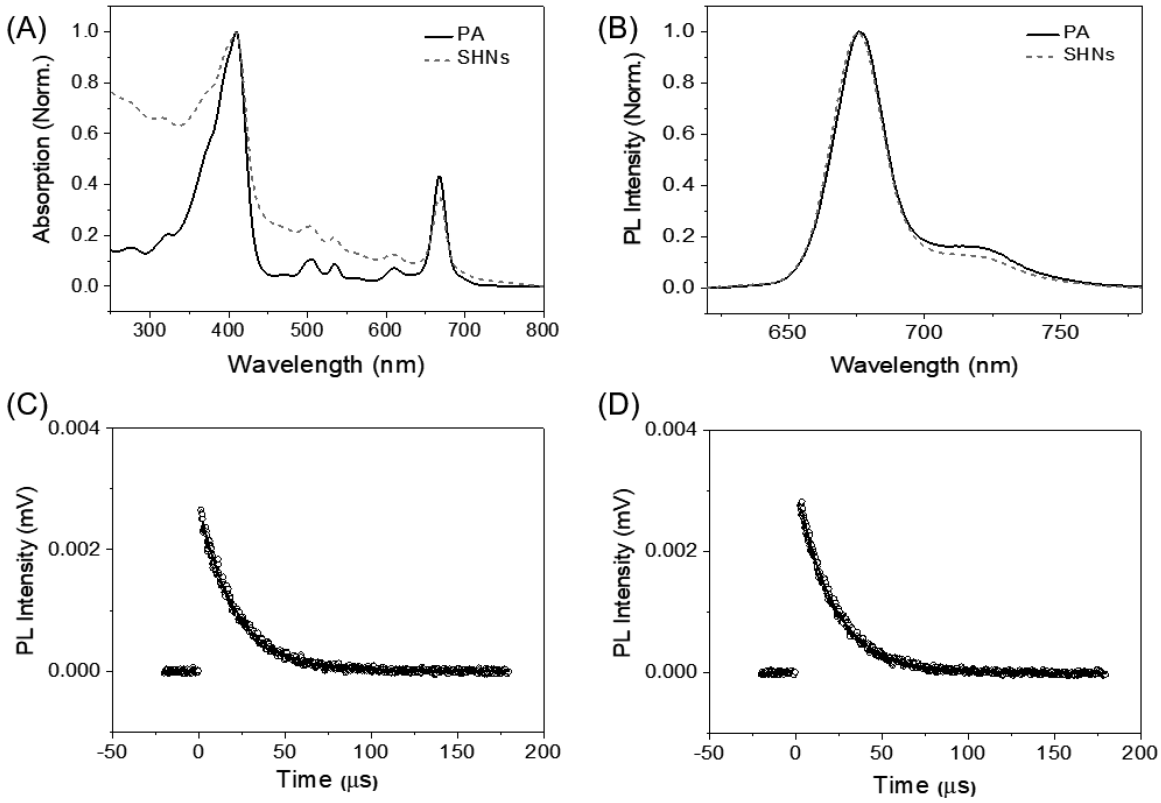


**Figure 3.** (A) Steady-state absorption and (B) emission spectra of PA molecules and SHNs in THF. The excitation wavelength is 410 nm for the emission spectra. Singlet oxygen phosphorescence decay signals from (C) PA and (D) SHNs in THF solution. The signals were detected at 1270 nm and fitted with a single exponential decay function (solid line).

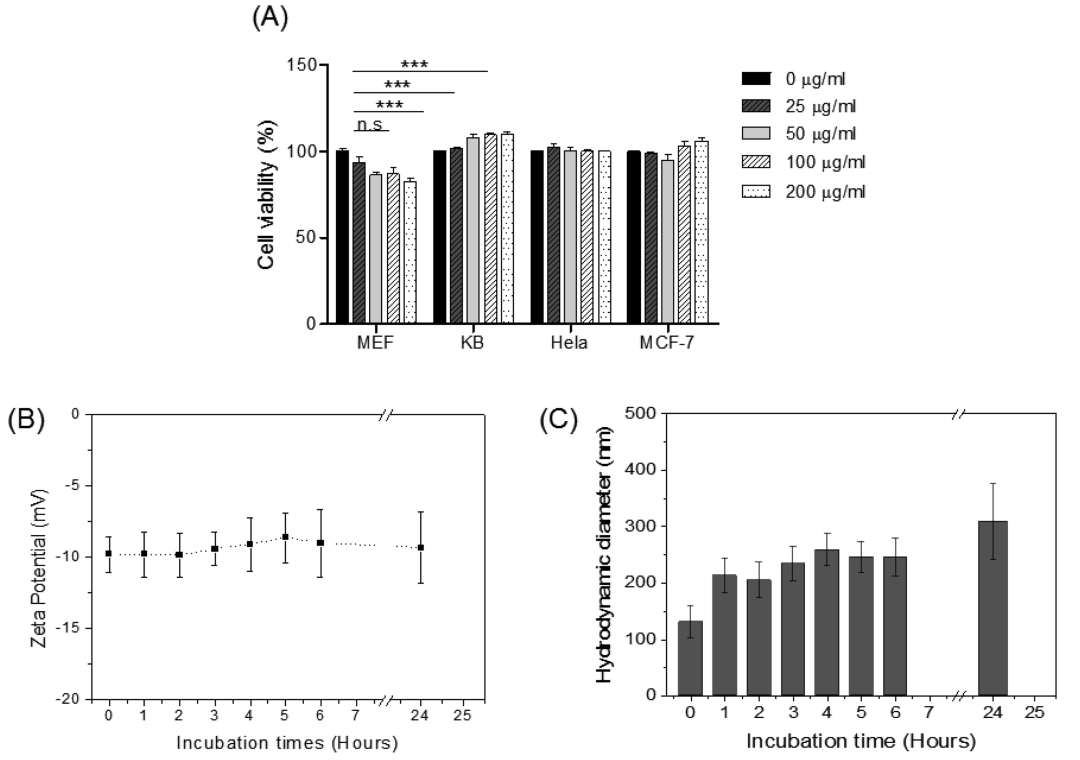


**Figure 4.** (A) Toxicity test of SHNs on MEF, KB, HeLa, and MCF-7 cells. (B) Polarity and (C) hydrodynamic diameter of SHNs in DMEM containing 10% FBS solution. All experiments were repeated three times, and data were represented as means ± SD. ***$p < 0.001$ for one-way ANOVA.



DOI: 10.1021/acs.jpcb.9b04301
J. Phys. Chem. B XXXX, XXX, XXX−XXX

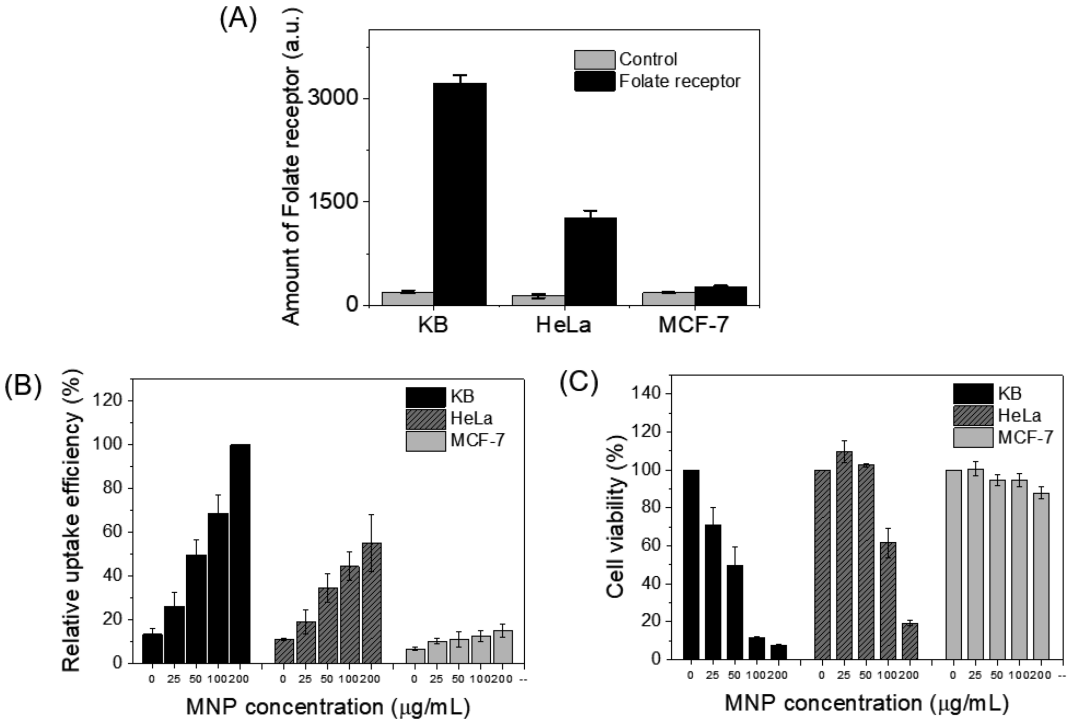


**Figure 5.** (A) Relative levels of FR expressed on the surface of indicated cancer cells assessed by flow cytometry. Mean fluorescence intensity (MFI) of each cell type incubated with isotype control antibody (gray bar) was set as 100% (B) Relative levels of cellular adsorption of SHNs by indicated cancer cells. MFI (>600 nm, based on PA emission spectra) emitted by KB cells incubated with 200 $\mu$g/mL of MNPs was set as 100%, and the relative MFIs from cells treated with the indicated conditions were compared. (C) Photodynamic inactivation efficiencies on indicated cancer cells depending on the concentration of incubated SHNs as assessed by cellular viability. All experiments were repeated three times.

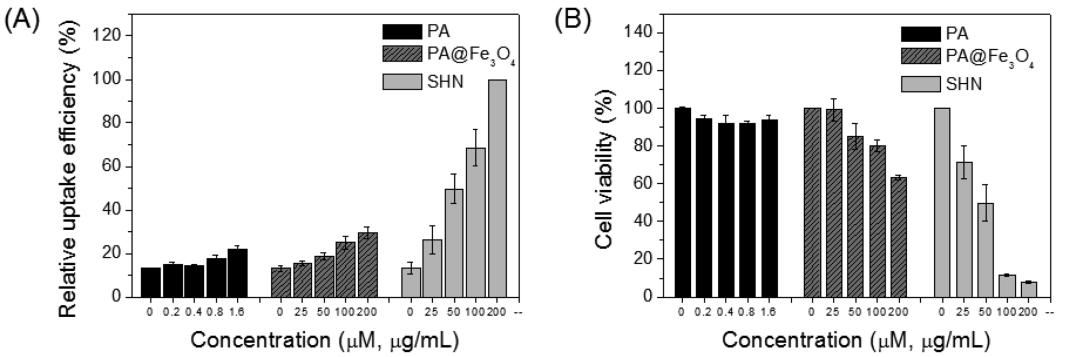


**Figure 6.** (A) Relative levels of cellular adsorption of free PA, PA@$Fe_3O_4$, or SHNs by KB cells. MFI (>600 nm, based on PA emission spectra) emitted by KB cells incubated with 200 $\mu$g/mL of MNPs was set as 100%, and the relative MFIs from cells treated with the indicated conditions were compared. (B) Photodynamic inactivation efficiencies of KB cells depending on the concentration of PA, PA@$Fe_3O_4$, or SHNs incubated. All experiments were repeated three times.

size increase of SHNs can be possibly due to the hard protein corona formed on the surface of SHN.[50,51]

KB, HeLa, and MCF-7 cells were used to check the selectivity of SHN for the PDI effect. The expression level of folate receptor on the surface of KB, HeLa, and MCF-7 cells was analyzed by flow cytometry. As in Figure 5A, KB cells express the highest level of FRs on the surface, whereas the expression of FRs on MCF-7 cells was not significant.[52] The more efficient uptake of SHNs to KB cells is observed compared with HeLa and MCF-7 cell as shown in Figure 5B and in Supporting Information Figure 1, which correlated well with the expression levels of FRs on the surface of cancer cell types. Moreover, the uptake amount of SHNs to KB and HeLa cells linearly increases, depending on the concentration of the incubated SHNs. This suggests that SHN can be applied for the targeting and the sensing of specific cancer cell types with high levels of FRs. Consistently, cellular viabilities of FR-positive KB and HeLa cells after photodynamic treatment significantly decreased as the concentration of incubated SHNs was increased, whereas those of FR-negative MCF-7 cells were not significantly changed (Figure 5C). These results clearly suggest that PDI efficiency by SHN is dependent on the expression levels of FRs on cancer cells.

Finally, in order to confirm the selective PDI effect by SHNs, KB cells were incubated with free PA molecules, PA@$Fe_3O_4$, and SHNs and exposed to LED light for the PDI effect after washing the cells to remove the nonadsorbed molecules. As shown in Figure 6, SHNs were more efficiently adsorbed by


DOI: 10.1021/acs.jpcb.9b04301
J. Phys. Chem. B XXXX, XXX, XXX−XXX

KB cells than PA or PA@$Fe_3O_4$, and the PDI efficiency was more dramatically enhanced by SHNs in a concentration-dependent manner. In the case of PA@$Fe_3O_4$, the viability of the KB cell was also moderately decreased depending on the increasing concentration of PA@$Fe_3O_4$. This result might be due to nonspecific adsorption of PA@$Fe_3O_4$ by KB cells as reported previously.[54−56]

## CONCLUSIONS

For the selective PDI treatment of FR-positive cancer cells, we have designed and fabricated target-oriented MNPs coated with PA as photosensitizer and FA as FR-targeting ligand. This shows low cytoxicity and endurable stability in cell culture media without loss of the original functionality of generating ROS and targeting the FR-positive cancer cell type. Moreover, the self-quenching effect of singlet oxygen generated by SHNs was negligible. PDI treatment of various cancer cell types including KB, HeLa, and MCF-7 cells with SHNs showed that KB cells with the highest level of FR expression on the surface were most efficiently killed by PDI at a lower dosage range of SHNs than others, suggesting an FR-dependent targeting by SHNs. Therefore, SHNs can be utilized as a magnetic PDI reagent for the selective treatment against FR-positive cancers.

## ASSOCIATED CONTENT

### Supporting Information

The Supporting Information is available free of charge on the ACS Publications website at DOI: 10.1021/acs.jpcb.9b04301.

Fluorscence images and FACS data of SHN on cancer cells (PDF)

## AUTHOR INFORMATION


### Corresponding Authors

*E-mail: yrkim@yonsei.ac.kr. Phone: +82-2-2123-2646. Fax: +82-2-364-7050.

*E-mail: kara1905@yonsei.ac.kr. Phone: +82-2-2123-7526. Fax: +82-2-364-7050.

*E-mail: chonh@snu.ac.kr. Phone: +82-2-740-8392. Fax: +82-2-743-0881.

### ORCID

Yong-Rok Kim: 0000-0001-8166-9889

### Author Contributions

⊥J.-W. Hwang, T.-J. Cheong, S.-J. Jung, and Y. Kim contributed equally to this manuscript.


### Notes

The authors declare no competing financial interest.

## ACKNOWLEDGMENTS

This work was supported by the National Research Foundation of Korea (NRF) grant funded by the Korea government (MSIP) (NRF-2017R1A5A1015365, NRF-2016R1A2B4011155), Republic of Korea.

## REFERENCES


(1) Robertson, C. A.; Evans, D. H.; Abrahamse, H. Photodynamic Therapy (PDT): A Short Review on Cellular Mechanisms and Cancer Research Applications for PDT. *J. Photochem. Photobiol., B* **2009**, *96*, 1−8.

(2) Dolmans, D. E.; Fukumura, D.; Jain, R. K. Photodynamic Therapy for Cancer. *Nat. Rev. Cancer* **2003**, *3*, 380−387.

(3) Saneesh Babu, P. S.; Manu, P. M.; Dhanya, T. J.; Tapas, P.; Meera, R. N.; Surendran, A.; Aneesh, K. A.; Vadakkancheril, S. J.; Ramaiah, D.; Nair, S. A.; et al. Bis(3,5-diiodo-2,4,6-trihydroxyphenyl)-squaraine Photodynamic Therapy Disrupts Redox Homeostasis and Induce Mitochondria-mediated Apoptosis in Human Breast Cancer Cells. *Sci. Rep.* **2017**, *7*, 42126.

(4) Jarvi, M. T.; Niedre, M. J.; Patterson, M. S.; Wilson, B. C. Singlet Oxygen Luminescence Dosimetry (SOLD) for Photodynamic Therapy: Current Status, Challenges and Future Prospects. *Photochem. Photobiol.* **2006**, *82*, 1198−1210.

(5) Chen, M. H.; Jenh, Y. J.; Wu, S. K.; Chen, Y. S.; Hanagata, N.; Lin, F. H. Non-invasive Photodynamic Therapy in Brain Cancer by Use of $Tb^{3+}$-Doped $LaF_3$ Nanoparticles in Combination with Photosensitizer Through X-ray Irradiation: A Proof-of-Concept Study. *Nanoscale Res. Lett.* **2017**, *12*, 62.

(6) Agostinis, P.; Berg, K.; Cengel, K. A.; Foster, T. H.; Girotti, A. W.; Gollnick, S. O.; Hahn, S. M.; Hamblin, M. R.; Juzeniene, A.; Kessel, D.; et al. Photodynamic Therapy of Cancer: An Update. *Ca-Cancer J. Clin.* **2011**, *61*, 250−281.

(7) Triesscheijn, M.; Baas, P.; Schellens, J. H.; Stewart, F. A. Photodynamic Therapy in Oncology. *Oncologist* **2006**, *11*, 1034−1044.

(8) Walther, J.; Schastak, S.; Dukic-Stefanovic, S.; Wiedemann, P.; Neuhaus, J.; Claudepierre, T. Efficient Photodynamic Therapy on Human Retinoblastoma Cell Lines. *PLoS One* **2014**, *9*, e87453.

(9) Ueki, N.; Lee, S.; Sampson, N. S.; Hayman, M. J. Selective Cancer Targeting with Prodrugs Activated by Histone Deacetylases and a Tumour-Associated Protease. *Nat. Commun.* **2013**, *4*, 2735.

(10) Jia, N. Y.; Zhang, S. J.; Shao, P.; Bagia, C.; Janjic, J. M.; Ding, Y.; Bai, M. F. Cannabinoid CB2 Receptor as a New Phototherapy Target for the Inhibition of Tumor Growth. *Mol. Pharmaceutics* **2014**, *11*, 1919−1929.

(11) Au, L.; Zhang, Q.; Cobley, C. M.; Gidding, M.; Schwartz, A. G.; Chen, J.; Xia, Y. Quantifying the Cellular Uptake of Antibody-Conjugated Au Nanocages by Two-Photon Microscopy and Inductively Coupled Plasma Mass Spectrometry. *ACS Nano* **2010**, *4*, 35−42.

(12) Chen, R.; Wang, X.; Yao, X.; Zheng, X.; Wang, J.; Jiang, X. Near-IR-Triggered Photothermal/Photodynamic Dual-Modality Therapy System via Chitosan Hybrid Nanospheres. *Biomaterials* **2013**, *34*, 8314−8322.

(13) Pereira, P. M.; Korsak, B.; Sarmento, B.; Schneider, R. J.; Fernandes, R.; Tome, J. P. Antibodies Armed with Photosensitizers: from Chemical Synthesis to Photobiological Applications. *Org. Biomol. Chem.* **2015**, *13*, 2518−2529.

(14) Serebrovskaya, E. O.; Edelweiss, E. F.; Stremovskiy, O. A.; Lukyanov, K. A.; Chudakov, D. M.; Deyev, S. M. Targeting Cancer Cells by Using an Antireceptor Antibody-Photosensitizer Fusion Protein. *Proc. Natl. Acad. Sci. U. S. A.* **2009**, *106*, 9221−9225.

(15) Hussain, A. F.; Kampmeier, F.; von Felbert, V.; Merk, H. F.; Tur, M. K.; Barth, S. SNAP-Tag Technology Mediates Site Specific Conjugation of Antibody Fragments with a Photosensitizer and Improves Target Specific Phototoxicity in Tumor Cells. *Bioconjugate Chem.* **2011**, *22*, 2487−2495.

(16) Yin, Y.; Zhu, W. W.; Guo, L. P.; Yang, R.; Li, X. S.; Jiang, Y. RGDC Functionalized Titanium Dioxide Nanoparticles Induce Less Damage to Plasmid DNA but Higher Cytotoxicity to HeLa Cells. *J. Phys. Chem. B* **2013**, *117*, 125−131.

(17) Chan, M. H.; Chen, S. P.; Chen, C. W.; Chan, Y. C.; Lin, R. J.; Tsai, D. P.; Hsiao, M.; Chung, R.-J.; Chen, X.; Liu, R. S. Single 808 nm Laser Treatment Comprising Photothermal and Photodynamic Therapies by Using Gold Nanorods Hybrid Upconversion Particles. *J. Phys. Chem. C* **2018**, *122*, 2402−2412.

(18) Robinson-Duggon, J.; Pérez-Mora, F.; Valverde-Vásquez, L.; Cortés-Arriagada, D.; De la Fuente, J. R.; Günther, G.; Fuentealba, D. Supramolecular Reversible On-Off Switch for Singlet Oxygen Using Cucurbit[n]uril Inclusion Complexes. *J. Phys. Chem. C* **2017**, *121*, 21782−21789.

(19) Baumann, P.; Spulber, M.; Dinu, I. A.; Palivan, C. G. Cellular Trojan Horse Based Polymer Nanoreactors with Light-Sensitive Activity. *J. Phys. Chem. B* **2014**, *118*, 9361−9370.




DOI: 10.1021/acs.jpcb.9b04301
J. Phys. Chem. B XXXX, XXX, XXX−XXX

(20) Huang, X.; Tian, X. J.; Yang, W. L.; Ehrenberg, B.; Chen, J. Y. The Conjugates of Gold Nanorods and Chlorin e6 for Enhancing the Fluorescence Detection and Photodynamic Therapy of Cancers. *Phys. Chem. Chem. Phys.* **2013**, *15*, 15727−15733.
(21) Lundqvist, M.; Stigler, J.; Cedervall, T.; Berggard, T.; Flanagan, M. B.; Lynch, I.; Elia, G.; Dawson, K. The Evolution of the Protein Corona around Nanoparticles: A Test Study. *ACS Nano* **2011**, *5*, 7503−7509.
(22) Safi, M.; Courtois, J.; Seigneuret, M.; Conjeaud, H.; Berret, J. F. The Effects of Aggregation and Protein Corona on the Cellular Internalization of Iron Oxide Nanoparticles. *Biomaterials* **2011**, *32*, 9353−9363.
(23) Mirshafiee, V.; Mahmoudi, M.; Lou, K. Y.; Cheng, J. J.; Kraft, M. L. Protein Corona Significantly Reduces Active Targeting Yield. *Chem. Commun.* **2013**, *49*, 2557−2559.
(24) Fleischer, C. C.; Payne, C. K. Nanoparticle Surface Charge Mediates the Cellular Receptors Used by Protein-Nanoparticle Complexes. *J. Phys. Chem. B* **2012**, *116*, 8901−8907.
(25) Jedlovszky-Hajdu, A.; Bombelli, F. B.; Monopoli, M. P.; Tombacz, E.; Dawson, K. A. Surface Coatings Shape the Protein Corona of SPIONs with Relevance to Their Application In vivo. *Langmuir* **2012**, *28*, 14983−14991.
(26) Sun, T. M.; Zhang, Y. S.; Pang, B.; Hyun, D. C.; Yang, M. X.; Xia, Y. N. Engineered Nanoparticles for Drug Delivery in Cancer Therapy. *Angew. Chem., Int. Ed.* **2014**, *53*, 12320−12364.
(27) Shang, L.; Nienhaus, K.; Nienhaus, G. U. Engineered Nanoparticles Interacting with Cells: Size Matters. *J. Nanobiotechnol.* **2014**, *12*, 5.
(28) Zhang, S. L.; Li, J.; Lykotrafitis, G.; Bao, G.; Suresh, S. Size-Dependent Endocytosis of Nanoparticles. *Adv. Mater.* **2009**, *21*, 419−424.
(29) Chen, D. Z.; Tang, Q. S.; Li, X. D.; Zhou, X. J.; Zang, J.; Xue, W. Q.; Xiang, J. Y.; Guo, C. Q. Biocompatibility of Magnetic $Fe_3O_4$ Nanoparticles and Their Cytotoxic Effect on MCF-7 Cells. *Int. J. Nanomed.* **2012**, *7*, 4973−4982.
(30) Mahdavi, M.; Ahmad, M. B.; Haron, M. J.; Namvar, F.; Nadi, B.; Rahman, M. Z.; Amin, J. Synthesis, Surface Modification and Characterization of Biocompatible Magnetic Iron Oxide Nanoparticles for Biomedical Applications. *Molecules* **2013**, *18*, 7533−7548.
(31) Ge, R.; Li, X.; Lin, M.; Wang, D.; Li, S.; Liu, S.; Tang, Q.; Liu, Y.; Jiang, J.; Liu, L.; et al. $Fe_3O_4$@polydopamine Composite Theranostic Superparticles Employing Preassembled $Fe_3O_4$ Nanoparticles as the Core. *ACS Appl. Mater. Interfaces* **2016**, *8*, 22942−22952.
(32) Du, S. W.; Zhang, L. K.; Han, K.; Chen, S.; Hu, Z.; Chen, W.; Hu, K.; Yin, L.; Wu, B.; Guan, Y. Q. Combined Phycocyanin and Hematoporphyrin Monomethyl Ether for Breast Cancer Treatment via Photosensitizers Modified $Fe_3O_4$ Nanoparticles Inhibiting the Proliferation and Migration of MCF-7 Cells. *Biomacromolecules* **2018**, *19*, 31−41.
(33) Choi, K. H.; Lee, H. J.; Park, B. J.; Wang, K. K.; Shin, E. P.; Park, J. C.; Kim, Y. K.; Oh, M. K.; Kim, Y. R. Photosensitizer and Vancomycin-Conjugated Novel Multifunctional Magnetic Particles as Photoinactivation Agents for Selective Killing of Pathogenic Bacteria. *Chem. Commun.* **2012**, *48*, 4591−4593.
(34) Wang, K. K.; Jung, S. J.; Hwang, J. W.; Kim, B. J.; Kim, D. H.; Bae, I. K.; Jeong, S. H.; Kim, Y. R. Bactericidal Effect Through Non-Uptake Pathway with Photofunctional Silicon Polymer that Generates Reactive Oxygen Species. *J. Photochem. Photobiol., A* **2016**, *315*, 52−58.
(35) Wang, K. K.; Shin, E. P.; Lee, H. J.; Jung, S. J.; Hwang, J. W.; Heo, I.; Kim, J. H.; Oh, M. K.; Kim, Y. R. Target-Oriented Photofunctional Nanoparticles (TOPFNs) for Selective Photodynamic Inactivation of Methicillin-Resistant Staphylococcus Aureus (MRSA). *J. Photochem. Photobiol., B* **2018**, *183*, 184−190.
(36) Zhang, Q.; Liu, J.; Yuan, K.; Zhang, Z.; Zhang, X.; Fang, X. A Multi-Controlled Drug Delivery System Based on Magnetic Mesoporous $Fe_3O_4$ Nanoparticles and a Phase Change Material for Cancer Thermo-Chemotherapy. *Nanotechnology* **2017**, *28*, 405101.
(37) Ursini, C. L.; Cavallo, D.; Fresegna, A. M.; Ciervo, A.; Maiello, R.; Tassone, P.; Buresti, G.; Casciardi, S.; Iavicoli, S. Evaluation of Cytotoxic, Genotoxic and Inflammatory Response in Human Alveolar and Bronchial Epithelial Cells Exposed to Titanium Dioxide Nanoparticles. *J. Appl. Toxicol.* **2014**, *34*, 1209−1219.
(38) Min, C. K.; Kim, H. I.; Ha, N. Y.; Kim, Y.; Kwon, E. K.; Yen, N. T. H.; Youn, J. I.; Jeon, Y. K.; Inn, K. S.; Choi, M. S.; et al. A Type I Interferon and IL-10 Induced by Orientia tsutsugamushi Infection Suppresses Antigen-Specific T Cells and Their Memory Responses. *Front. Immunol.* **2018**, *9*, 2022.
(39) Leamon, C. P.; Low, P. S. Delivery of Macromolecules into Living Cells: A Method that Exploits Folate Receptor Endocytosis. *Proc. Natl. Acad. Sci. U. S. A.* **1991**, *88*, 5572−5576.
(40) Figini, M.; Ferri, R.; Mezzanzanica, D.; Bagnoli, M.; Luison, E.; Miotti, S.; Canevari, S. Reversion of Transformed Phenotype in Ovarian Cancer Cells by Intracellular Expression of Antifolate Receptor Antibodies. *Gene Ther.* **2003**, *10*, 1018−1025.
(41) Wang, X.; Li, J.; Wang, Y.; Koenig, L.; Gjyrezi, A.; Giannakakou, P.; Shin, E. H.; Tighiouart, M.; Chen, Z. G.; Nie, S.; Shin, D. M. A Folate Receptor-Targeting Nanoparticle Minimizes Drug Resistance in a Human Cancer Model. *ACS Nano* **2011**, *5*, 6184−6194.
(42) Gerlier, D.; Thomasset, N. Use of MTT Colorimetric Assay to Measure Cell Activation. *J. Immunol. Methods* **1986**, *94*, 57−63.
(43) Freimoser, F. M.; Jakob, C. A.; Aebi, M.; Tuor, U. The MTT [3-(4,5-dimethylthiazol-2-yl)-2,5-diphenyltetrazolium bromide] Assay is a Fast and Reliable Method for Colorimetric Determination of Fungal Cell Densities. *Appl. Environ. Microbiol.* **1999**, *65*, 3727−3729.
(44) Huang, Y. N.; Zhang, L. P.; Huan, W. W.; Liang, X. J.; Liu, X. N.; Yang, Y. X. A Study on Synthesis and Properties of $Fe_3O_4$ Nanoparticles by Solvothermal Method. *Glass Phys. Chem.* **2010**, *36*, 325−331.
(45) Xiao, Y.; Lin, Z. T.; Chen, Y.; Wang, H.; Deng, Y. L.; Le, D. E.; Bin, J.; Li, M.; Liao, Y.; Liu, Y.; et al. High Molecular Weight Chitosan Derivative Polymeric Micelles Encapsulating Superparamagnetic Iron Oxide for Tumor-Targeted Magnetic Resonance Imaging. *Int. J. Nanomed.* **2015**, *10*, 1155−1172.
(46) Nair K, L.; Jagadeeshan, S.; Nair S, A.; Kumar, G. S. Folic Acid Conjugated Delta-valerolactone-poly(ethylene glycol) Based Triblock Copolymer as a Promising Carrier for Targeted Doxorubicin Delivery. *PLoS One* **2013**, *8*, e70697.
(47) Wu, N. Q.; Fu, L.; Su, M.; Aslam, M.; Wong, K. C.; Dravid, V. P. Interaction of Fatty Acid Monolayers with Cobalt Nanoparticles. *Nano Lett.* **2004**, *4*, 383−386.
(48) Wang, K. K.; Jang, J. W.; Shin, E. P.; Song, H. W.; Hwang, J. W.; Kim, Y. K.; Lim, C. S.; Kim, Y. R. Eradication of Plasmodium Falciparum from Erythrocytes by Controlled Reactive Oxygen Species via Photodynamic Inactivation Coupled with Photofunctional Nanoparticles. *ACS Appl. Mater. Interfaces* **2017**, *9*, 12975−12981.
(49) Huang, P.; Li, Z.; Lin, J.; Yang, D.; Gao, G.; Xu, C.; Bao, L.; Zhang, C.; Wang, K.; Song, H.; et al. Photosensitizer-Conjugated Magnetic Nanoparticles for In Vivo Simultaneous Magnetofluorescent Imaging and Targeting Therapy. *Biomaterials* **2011**, *32*, 3447−3458.
(50) Fleischer, C. C.; Payne, C. K. Nanoparticle-Cell Interactions: Molecular Structure of the Protein Corona and Cellular Outcomes. *Acc. Chem. Res.* **2014**, *47*, 2651−2659.
(51) Whitwell, H.; Mackay, R. M.; Elgy, C.; Morgan, C.; Griffiths, M.; Clark, H.; Skipp, P.; Madsen, J. Nanoparticles in the Lung and Their Protein Corona: The Few Proteins That Count. *Nanotoxicology* **2016**, *10*, 1385−1394.
(52) Lundqvist, M.; Augustsson, C.; Lilja, M.; Lundkvist, K.; Dahlback, B.; Linse, S.; Cedervall, T. The Nanoparticle Protein Corona Formed in Human Blood or Human Blood Fractions. *PLoS One* **2017**, *12*, e0175871.
(53) Suzuki, H.; Toyooka, T.; Ibuki, Y. Simple and Easy Method to Evaluate Uptake Potential of Nanoparticles in Mammalian Cells Using a Flow Cytometric Light Scatter Analysis. *Environ. Sci. Technol.* **2007**, *41*, 3018−3024.


DOI: 10.1021/acs.jpcb.9b04301
J. Phys. Chem. B XXXX, XXX, XXX−XXX

(54) Hu, F.; MacRenaris, K. W.; Waters, E. A.; Liang, T.; Schultz-Sikma, E. A.; Eckermann, A. L.; Meade, T. J. Ultrasmall, Water-Soluble Magnetite Nanoparticles with High Relaxivity for Magnetic Resonance Imaging. *J. Phys. Chem. C* **2009**, *113*, 20855−20860.
(55) Klein, S.; Sommer, A.; Distel, L. V. R.; Hazemann, J. L.; Kröner, W.; Neuhuber, W.; Müller, P.; Proux, O.; Kryschi, C. Superparamagnetic Iron Oxide Nanoparticles as Novel X-ray Enhancer for Low-Dose Radiation Therapy. *J. Phys. Chem. B* **2014**, *118*, 6159−6166.
(56) de Sousa, M. E.; Carrea, A.; Mendoza Zélis, P. M.; Muraca, D.; Mykhaylyk, O.; Sosa, Y. E.; Goya, R. G.; Sánchez, F. H.; Dewey, R. A.; Fernandez van Raap, M. B. F. Stress-Induced Gene Expression Sensing Intracellular Heating Triggered by Magnetic Hyperthermia. *J. Phys. Chem. C* **2016**, *120*, 7339−7348.


DOI: 10.1021/acs.jpcb.9b04301
*J. Phys. Chem. B* XXXX, XXX, XXX−XXX